Analyse d'un thermosiphon fermé diphasique utilisant de l'eau à pression subatmosphérique

Two-phase closed thermosiphon analysis using water at subatmospheric pressure

Frédy Abadassi [1,*], Ahmed G. Rahma [b], Pierre François[2], Fabrice Lawniczak [2], Abdellah Ghenaim[1], Abdelali Terfous [2], Abderahmane Marouf [2], Denis Funfschilling [2]

[1]INSA Strasbourg, ICube, UMR CNRS 7357, 67000 Strasbourg, France

[2] Université de Strasbourg ICube, UMR CNRS 7357, 67000 Strasbourg, France

[*](Corresponding author : fredy.abadassi@insa-strabourg.fr)

Résumé - Cette étude examine les performances thermiques d'un thermosiphon fermé diphasique en cuivre, rempli d'eau distillée et fonctionnant à pression subatmosphérique. Des expériences ont été menées avec un taux de remplissage de 80% et des puissances thermiques comprises entre 40,9 W et 201,9 W, tout en maintenant la température de refroidissement à 25 °C. L'analyse se concentre sur les coefficients d'échange thermique au niveau de l'évaporateur et du condenseur, ainsi que sur la résistance thermique globale. À faibles puissances, d'importantes oscillations dues à un phénomène d'ébullition de type geyser sont observées dans l'évaporateur. Ces instabilités diminuent à mesure que la puissance augmente, conduisant à un régime de fonctionnement plus stable.

Abstract - This study examines the thermal performance of a copper two-phase closed thermosiphon filled with distilled water and operated under subatmospheric pressure. Experiments were carried out at an 80% filling ratio with heat inputs ranging from 40.9 W to 201.9 W and a constant cooling temperature of 25 °C. The analysis focuses on heat transfer coefficients at the evaporator and condenser, as well as overall thermal resistance. At low heat inputs, significant oscillations due to geyser boiling are observed in the evaporator. These instabilities decreases as the heat input increases, leading to quasi-stable operating regime.

Nomenclature

A	cross-sectional area m^2	*Greek symbols*	
Q_{in}	heat input, W	σ	surface tension, $\mathrm{N/m}$
Q_{loss}	heat loss, W	*Index and exponent*	
q_{net}	Net heat flux, $\mathrm{W/m^2}$	eva	evaporator
T	temperature, K	con	condenser
h	heat transfer coefficient, $\mathrm{W/m^2.K}$	l	liquid
R_{th}	thermal resistance, $\mathrm{K/W}$	v	vapor

1 Introduction

The energy consumption of data centers (DCs) corresponds approximately to 1.6 to 2% of the global energy consumption, with a constant annual growth rate of 3.8% since 2018, as reported by the International

https://doi.org/10.25855/SFT2026-135

Fluid	T_{sat} [°C]	P [bar]	σ [mN/m]	ρ_l [kg/m^3]	ρ_v [kg/m^3]	h_{fg} [kJ/kg]	μ [Pa.s]
Water	30	0.042	71.19	995.61	0.030	2430	0.00079
	50	0.124	67.94	988.00	0.083	2382	0.00054
	80	0.470	62.67	971.77	0.290	2308	0.00035
	100	1.010	58.90	958.35	0.600	2256	0.00028

TABLE 1 – *Thermophysical properties of water at different saturation temperatures.*

Energy Agency (IEA) [1] due to the rapid growth of many technologies such as artificial intelligence (AI), social networking, gaming [2, 3]. In general, about 30 to 50% of the total energy consumption of a DC is dedicated to cooling [4]. The Two-Phase Thermosiphon (TPT) is an energy efficient, passive cooling technology for medium to high power applications, particularly in electronics and DCs [5-7]. It relies on gravity-assisted circulation : liquid evaporates in the evaporator, the resulting vapor rises to the condenser, and the condensed liquid returns downward under gravity, enabling a continuous cycle. TPTs are classified into two types : the Two-Phase Closed Thermosiphon (TPCT), consisting of a sealed tube, and the Two-Phase Loop Thermosiphon (TPLT), which features a loop with separate riser and downcomer sections [8].

Many experimental, numerical and theoretical studies have been carrying out on different aspect of the TPT, particularly on TPCT through the analysis of parameters including the heat flux, working fluid, inclination angle, operating pressure, geometrical parameters and the filling ratio (FR) of the working fluid, which is the volume of the liquid divided by the volume of the evaporator or the total internal volume of the tube [9, 10]. Working fluid effect in TPCT is one of the main subject investigated by researchers in the literature regarding two-phase thermosiphon heat exchanger operating principle. With the progressive phase-out of numerous refrigerants regulated by the Montreal Protocol, the Kigali Amendment, and current European legislation, recent research has increasingly focused on alternative fluids to replace conventional refrigerants such as Chlorofluorocarbons (CFCs), Hydrochlorofluorocarbons (HCFCs) and Hydrofluorocarbons (HFCs).

Previous investigations [11, 12] have shown that water provides higher heat-transfer coefficients, enhances maximum heat-transport capacity, and lower effective thermal resistance more than refrigerants such as Freon-11 and various dielectric fluids. Water aligns both with performance-driven criteria and with the global shift toward sustainable thermal management technologies. These considerations motivate the selection of water as the working fluid in the present study. Thermophysical properties of water are summarized in the table 1. Furthermore, geyser boiling in small-diameter TPCTs has been widely investigated in the literature [13, 14]. However, its inherent complexity makes it difficult to fully understand, particularly due to the influence of various physical and geometrical parameters. In the present study, this phenomenon was also observed and discussed.

2 Experimental setup and procedure

2.1 Experimental apparatus

Fig. 1 shows the schematic of the TPCT. The system consists of a vertical copper tube with a total length of 500 mm, an inner diameter of 20 mm, and a wall thickness of 1 mm. Copper was selected because

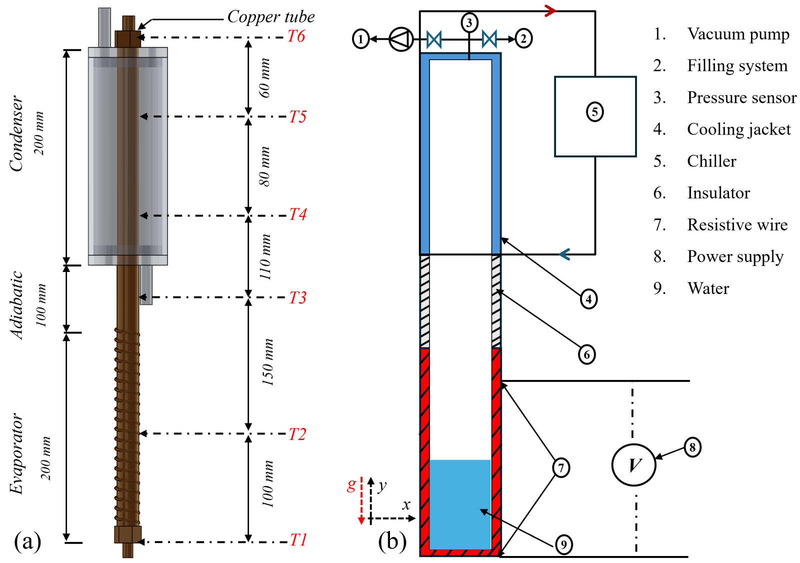

FIGURE 1 – *Schematic representation of the TPCT : (a) dimensions and locations of the monitoring points, (b) 2D schematic of the entire system.*

of its high thermal conductivity (λ = 401 W/m.K at 25 °C). The tube was divided into three parts such as the evaporator (bottom, 200 mm) that was heated with a resistive wire (10 Ω/m) connected to a power supply (Keysight E3634A), the adiabatic section (middle, 100 mm) , and the condenser (top, 200 mm) cooled by a circulating water loop with controlled temperature (cooling loop).

Six T-type thermocouples (Stainless steel 321, 18/8/1 Cr/Ni/Titanium-stabilized) were positioned along the copper tube to measure and monitor the temperature of the system (Fig. 1(a)). Thermocouple T1 was positioned inside the evaporator from the bottom of the tube and T6 inside the condenser section from the top. T2, T3, T4, and T5 measured the outer wall temperature at various locations. All thermocouples were connected to a data acquisition system (Agilent 34970A) via LabVIEW for automated recording. A piezoresistive pressure sensor was also installed at the top of the condenser to measure vapor pressure during the experiments.

2.2 Experimental procedure

A view of the experimental set up is shown in Fig. 2. Before charging, the copper tube was first cleaned through repeated rinsing with acetone followed by distilled water, then sealed tightly and vacuum-dried. Since the CPU have to be cooled at temperature lower than 55°C, and since we wanted to use water as green refrigerant fluid, the system were operated at subatmospheric pressure. More precisely, to avoid the presence of any other gases than water vapor who would not participate to the boiling and condensation cycle, the TPCT is completely vacuumed using a vacuum pump ILMVAC type 302103, before the introduction of liquid water (FR = 80%). As a result, the pressure in the TPCT is the saturation pressure corresponding to the temperature of the condenser. Following charging, the cooling temperature was settle up at the 25 °C using a chiller (Thermo Scientific ARCTIC A10 Refrigerated Circulators) with a volumetric flow rate of 17 L/min. The heat input in the evaporator was increased gradually, and six heat levels were tested such as 40.9 W, 79.3 W, 106.2 W 143.6 W, 178.5 W, 201.9 W corresponding respectively to the following heat flux : 3.25 kW/m^2, 6.31 kW/m^2, 8.45 kW/m^2, 11.43 kW/m^2, 14.21 kW/m^2, and 16.07 kW/m^2. After each adjustment, the system was allowed to reach steady state before proceeding to the next step.

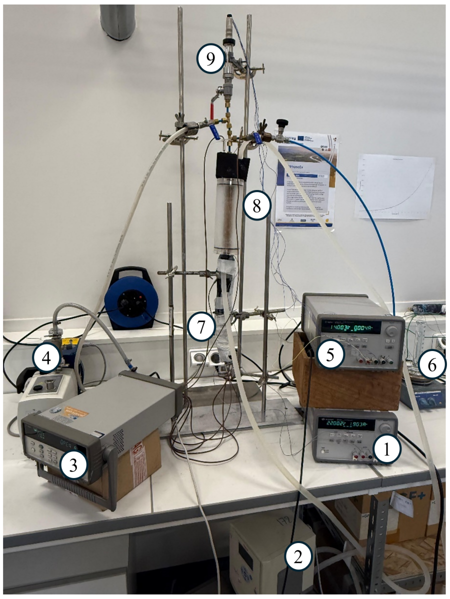

1. Heating power supply
2. Chiller
3. Data logger
4. Vacuum pump
5. Pressure sensor power supply
6. Filling device for water
7. Evaporator + Insulation
8. Cooling jacket
9. Pressure sensor

FIGURE 2 – *Photographs of the experimental set up.*

2.3 Data reduction

The heat input to the evaporator (Q_{in}) was determined from the voltage (U) and the current (I) supplied by the power supply ($Q_{\text{in}} = U \cdot I$). Heat losses were estimated experimentally using an empty thermosiphon while running the cooling loop, and found to be about 3% based on correlations with temperature difference. These losses (Q_{loss}) were subtracted from the input power to obtain the effective heat transfer rate, $Q_{\text{tot}} = Q_{\text{in}} - Q_{\text{loss}}$. The heat flux ($q_{\text{net}}$) can be calculated from the total effective heat and the surface of the evaporator (A_{eva}) as :

$$q_{\text{net}} = \frac{Q_{\text{tot}}}{A_{\text{eva}}} \tag{1}$$

The HTC of the evaporator (h_{eva}) is computed by the Eq. 2, which is well used in the literature [15].

$$h_{\text{eva}} = \frac{Q_{\text{tot}}}{A_{\text{eva}}(T_{\text{eva}} - T_{\text{ad}})} \tag{2}$$

where T_{eva}, and T_{ad} are, respectively, the wall temperature of the evaporator (T_2 in this experiment) and the wall adiabatic section temperature (T_3) corresponding to vapor temperature.

To evaluate the heat transfer coefficient of the condenser (h_{con}), the following equation was used :

$$h_{\text{con}} = \frac{Q_{\text{tot}}}{A_{\text{con}}(T_{\text{ad}} - T_{\text{con}})} \tag{3}$$

where T_{con} is the average wall temperature of the condenser determined by a linear interpolation taking into consideration the position of the thermocouple (T_4, T_5 and T_6 in this experiment) used to assess the temperature distribution of the condenser.

Thermal resistance provides the steady-state thermal performance of TPT. It is determined as Eq. 4 :

$$R_{\text{th}} = \frac{(T_{\text{eva}} - T_{\text{con}})}{Q_{\text{tot}}} \tag{4}$$

Measurement	Device	Experimental Uncertainty
Temperature	T-type thermocouple	± 0.5°C
Pressure	Piezoresistive pressure transmitter	± 0.1%
Power Input (U and I)	Keysight power supply	< 0.5%

TABLE 2 – *Experimental uncertainties of the equipments.*

The uncertainties of the measurement devices are listed in the table 2. The standard uncertainty to the calculated quantities was calculated according to the Eq. 5, [15]. x_i represents each variable on which the function f is dependent. The maximum relative expanded uncertainties of the evaporator heat transfer coefficient, the condensation heat transfer coefficient and the overall thermal resistance are 12.2%, 15.3% and 7%, respectively.

$$\Delta f = \sqrt{\sum_{i=1}^{n} \left(\frac{\partial f}{\partial x_i} \Delta x_i \right)^2} \tag{5}$$

3 Results and discussion

3.1 Temperature distribution

Fig. 3 shows the temperature distribution over time for the six heats input. Significant temperature fluctuations were observed at low heat input (40.9 W, 79.3 W, as shown in Fig. 3(a,b)) particularly at 40.9 W leading to a geyser boiling with a period around 90 seconds. When the heat input is low, the liquid gradually becomes superheated until a vapor bubble forms and rapidly expands. This expansion pushes the liquid upward toward the condenser, inducing rapid vapor condensation. The liquid then returns to the evaporator as a subcooled film. As it reheats and becomes superheated again, the geyser boiling cycle repeats. This phenomenon were consistently observed in the Fig. 3(a) at 40.9 W, which is further clarified in the Fig. 4(a) using the temperature variation of the outer wall of the evaporator. The confinement number (Co) is well applied in flow boiling field to characterized the degree of confinement in the TPCT. It is defined by Cornwell and Kew [16] as the following equation :

$$Co = \frac{\lambda_c}{D_i} = \frac{1}{D_i} \sqrt{\frac{\sigma}{(\rho_l - \rho_v) g}} \tag{6}$$

where D_i is the inner diameter of the thermosiphon. λ_c is the capillary length, which is proportional to the bubble departure diameter. σ, ρ_l, ρ_v, and g denote the surface tension of the working fluid, the liquid and vapor densities, and the gravitational acceleration, respectively. A larger TPCT diameter results in a smaller Co, which facilitates smooth circulation of the working fluid. Conversely, a smaller diameter increases the Co value, making fluid circulation within the TPCT more difficult.

At low heat input, slow wall heating delays nucleation and bubble dynamics. Growing bubbles push liquid upward toward the condenser, creating a temporary counter-gravity flow and confined regime associated with geyser boiling. The liquid then drains back to the evaporator under gravity, returning to an unconfined state. The "Intermittent confinement" illustrated in the Fig. 4(a) refers to a periodic, gravity-defying liquid motion that temporarily restricts the TPCT. In this regime, the TPCT alternates repeatedly between confined and unconfined states during operation demonstrating geyser boiling regime.

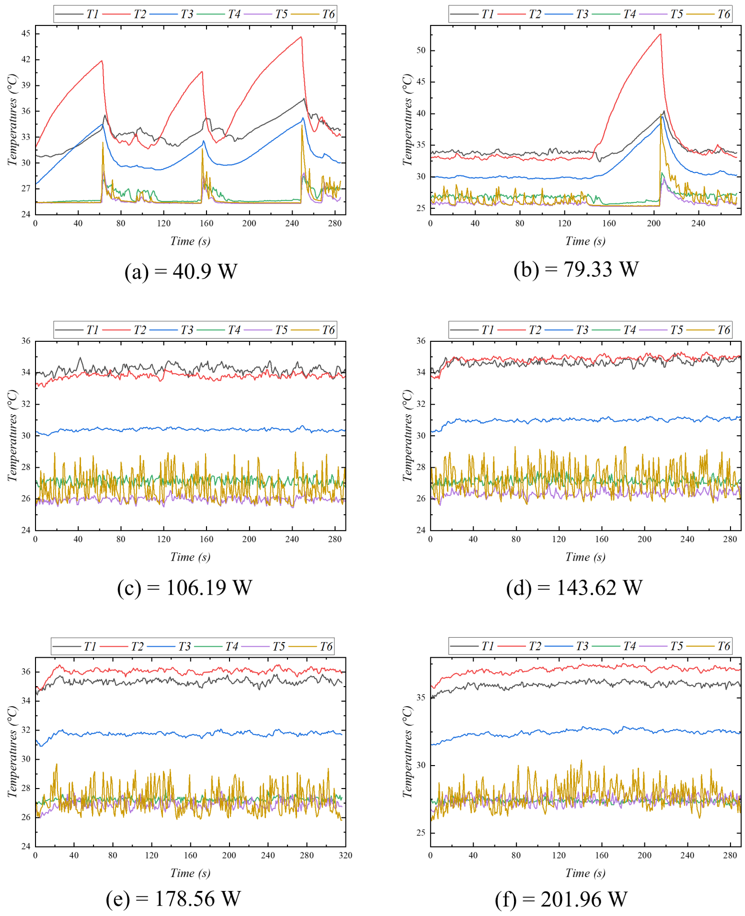

FIGURE 3 – *Temperature distribution over time at different heat input.*

The pressure fluctuations shown in Fig. 4 at low heat input reflect the thermal instability eventually associated with geyser boiling. As the heat input increases, the higher wall superheat promotes more nucleation, faster bubble growth, and quicker bubble departure. This behavior reduces the amplitude of temperature oscillations and leads to smoother circulation within the TPCT, as illustrated in Fig. 3 (c,f).

3.2 HTC of the evaporator and the condenser

Fig. 5(a) shows the HTC of the evaporator and the condenser. It shows that the first two heat flux levels (3.25, 6.31 kW/m²) correspond to an unstable operating regime dominated by geyser boiling. This regime is marked by strong temperature fluctuations at the evaporator wall and irregular variations in the HTC. From 8.45 kW/m² upward, including the 11.43, 14.21 and 16.07 kW/m², the evaporator response becomes more stable. The wall temperature distribution evens out, and the HTC approaches a nearly constant value with only minor oscillations. This transition indicates that higher heat input promotes more consistent nucleation and a more regular boiling process. On the other hand, the condenser HTC increases progressively from the lowest to the highest heat input. This trend indicates that higher heat input enhance the inertial forces of the circulating flow, thereby increasing the effective condensation surface and promoting more efficient heat transfer in the condenser.

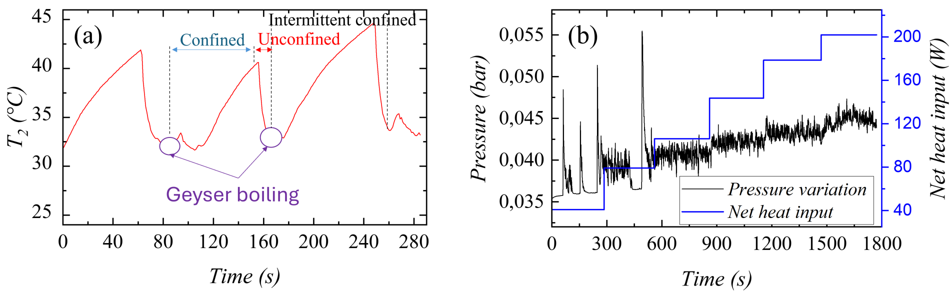

FIGURE 4 – *(a) Geyser boiling occurrence at low heat input, (b) Pressure variation over heat input.*

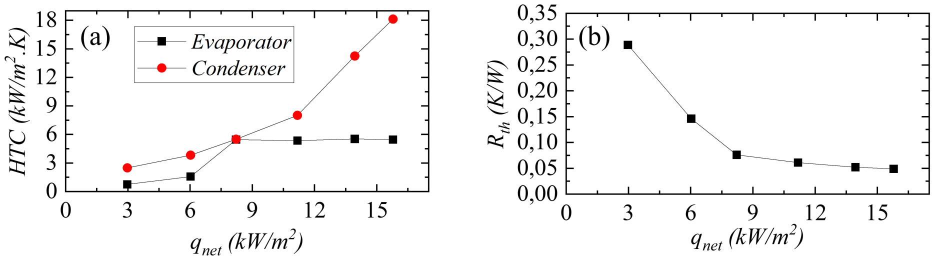

FIGURE 5 – *(a) HTC of the evaporator and condenser, (b) thermal resistance of the system.*

3.3 Thermal resistance

The thermal resistance of the TPCT decreases as the heat input increases (Fig. 5(b)), indicating the establishment of a stable pool boiling regime at higher power levels and a stable vapor liquid circulation throughout the system. This favorable behavior at high heat input, achieved in a small-diameter TPCT operating with water at low pressure with moderate FR (80%) and cooling temperature (25 °C), is highly promising for waste heat recovery applications in DCs.

4 Conclusion

This study experimentally investigated the thermal behavior of a small-diameter two-phase closed Thermosiphon operating with water at low operating pressure. The results show that at low heat inputs, the TPCT exhibits strong thermal instabilities characterized by intermittent confined flow and geyser boiling, leading to significant temperature and pressure fluctuations and reduced heat transfer performance. As the heat input increases, the system undergoes transition toward a stable boiling regime. These findings highlight the potential of small-diameter TPCTs, when properly optimized in terms of FR and cooling conditions, for effective waste heat recovery and thermal management in DCs applications.

References

1. (IEA), I. E. A. *Tracking data centres and data transmission networks 2020* `https://www.iea.org/energy-system/buildings/data-centres-and-data-transmission-networks, 2020`. Accessed 16-11-2025.

2. Haynau, R., Marcinichen, J. B., Amalfi, R. L., Cataldo, F. & Thome, J. R. *Thermosyphon simulation code: transient thermal performance and experimental validation* in *2021 20th IEEE Intersociety Conference on Thermal and Thermomechanical Phenomena in Electronic Systems (iTherm)* (2021).

3. Rahma, A. G. *et al.* Numerical assessment of condensation time relaxation coefficients for accurate prediction under atmospheric and subatmospheric conditions in two-phase thermosiphon systems. *International Journal of Heat and Mass Transfer* **252,** 127485 (2025).
4. Amalfi, R. L., Cataldo, F., Marcinichen, J. B. & Thome, J. R. *Experimental characterization of a server-level thermosyphon for high-heat flux dissipations* in *2020 19th IEEE Intersociety Conference on Thermal and Thermomechanical Phenomena in Electronic Systems (ITherm)* (2020), 402–409.
5. Rahma, A. G. *et al. Numerical Investigation of Condensation Time Relaxation Coefficients in Two-Phase Thermosiphon Systems for Low-Pressure Applications* in *26ème Congrès Français de Mécanique* (2025).
6. Cao, J. *et al.* A review on independent and integrated/coupled two-phase loop thermosyphons. *Applied Energy* **280,** 115885 (2020).
7. Abadassi, F. *et al. Thermal Characterization of a Two-Phase Closed Thermosyphon with Optimal Filling Ratio under Varying Condenser Temperatures.* in *Congrès Français de la Mécanique* (2025).
8. Rahma, A. G. *et al.* Two-phase thermosiphon cooling in data centers: a comprehensive review of refrigerants for practical selection. *Journal of Engineering and Applied Science* **72** (2025).
9. Smith, K., Kempers, R. & Robinson, A. Confinement and vapour production rate influences in closed two-phase reflux thermosyphons Part A: flow regimes. *International Journal of Heat and Mass Transfer* **119,** 907–921 (2018).
10. Rahma, A. *et al. Influence of Filling Ratio on Flow Pattern in a Two-Phase Closed Thermosiphon at Fixed Confinement Number* in *2025 4th International Conference on Electronic Engineering (ICEEM)* (2025), 1–6.
11. Sauciuc, I., Akbarzadeh, A. & Johnson, P. Characteristics of two-phase closed thermosiphons for medium temperature heat recovery applications. *Heat Recovery Systems and CHP* **15** (1995).
12. Rahma, A. *et al. Effect of Filling Ratio on Two-Phase Closed Thermosiphon Heat Transfer under Constant Confinement and Weber Number* in *2025 7th Novel Intelligent and Leading Emerging Sciences Conference (NILES)* (2025), 90–94.
13. Mantelli, M. B., Colle, S., de Carvalho, R. D. & de Moraes, D. U. *Study of closed two-phase thermosyphons for bakery oven application* tech. rep. (Cidade Univ. Trindade, Florianopolis, Santa Catarina (BR), 1999).
14. Casarosa, C., Latrofa, E. & Shelginski, A. The geyser effect in a two-phase thermosyphon. *International Journal of Heat and Mass Transfer* **26,** 933–941 (1983).
15. Kang, S., Lee, S. & Lee, J. Performance enhancement of two-phase closed thermosyphon with threaded evaporator surface. *International Communications in Heat and Mass Transfer* **164** (2025).
16. Cornwell, K. & Kew, P. A. in *Energy Efficiency in Process Technology* 624–638 (Springer, 1993).

Acknowledgment

The 2PhaseEx project is part of the Science Offensive of the trinational Upper Rhine Metropolitan Region, co-financed by the European Union via the Interreg Upper Rhine programme. The authors would also like to thank the MICROFLOTEC project for its valuable support and collaboration.